International Journal of Mass Spectrometry 293 (2010) 12–22

Contents lists available at ScienceDirect

International Journal of Mass Spectrometry

journal homepage: www.elsevier.com/locate/ijms

Multiply charged gas-phase NaAOT reverse micelles: Formation, encapsulation of glycine, and collision-induced dissociation

Yigang Fang, Andrew Bennett, Jianbo Liu*

Department of Chemistry and Biochemistry, Queens College and the Graduate Center of the City University of New York, 65-30 Kissena Blvd., Flushing, NY 11367, USA

ARTICLE INFO

Article history:
Received 24 December 2009
Received in revised form 15 March 2010
Accepted 16 March 2010
Available online 30 March 2010

Keywords:
Gas-phase reverse micelles
Electrospray ionization
Guided-ion beam tandem mass spectrometer
Collision-induced dissociation

ABSTRACT

We report a study of the generation and characterization of multiply charged, sodium bis(2-ethylhexyl) sulfosuccinate (NaAOT) aggregates in the gas phase, using electrospray ionization (ESI) guided-ion beam tandem mass spectrometry. It was found that distributions of gas-phase NaAOT aggregate size and charge are related to the surfactant states in electrosprayed solutions. ESI mass spectra of NaAOT/water/hexane reverse micellar solutions show the compositions of $[(NaAOT)_nNa_z]^{z+}$, with the aggregation number (n) and charge (z) increase with increasing water content in solution. In contrast, gas-phase aggregates from NaAOT monomers in solution have smaller aggregation numbers and lower charges. Gas-phase NaAOT aggregates of $n \geq 13$ could encapsulate one glycine molecule, and those of $n \geq 16$ could encapsulate two glycine molecules. Up to five glycine molecules could be accommodated in single aggregates of $n \geq 24$. Regardless of glycine encapsulation, no water molecules were detected within gas-phase NaAOT aggregates. Collision-induced dissociation (CID) was studied for mass-selected NaAOT aggregates with Xe, including measurements of product ion masses and CID cross-sections for both empty and glycine-encapsulating aggregates over the center-of-mass collision energy range of 0.1–8.0 eV. CID results provide a detailed probe of aggregate structures as well as the interactions between surfactants and the encapsulated glycine molecules. Specifically, the dependence of glycine encapsulation on aggregate size is observed in CID product ion mass spectra, too. The present study demonstrates that NaAOT surfactants are able to form reverse micelles in the gas phase, and gas-phase reverse micelles can act as nanometer-sized vehicles for transport of non-volatile biomolecules.

© 2010 Elsevier B.V. All rights reserved.

1. Introduction

Reverse micelles formed by surfactants are among the most interesting nanometric structures. They can be schematically represented as globular aggregates, with the surfactant hydrophilic polar heads oriented around an internal core and the hydrophobic chains forming the outer surface. Reverse micelles can be used for selective solubilization and reactions which exploit their nanometer size, unique combination of micro-environments, and membrane mimetic properties [1–5]. Traditionally, reverse micelles are generated in apolar solvents [2] or supercritical fluids [4]. However, reverse micelles also exist in marine aerosols [6] and upper tropospheric aerosols [7], in which organic materials (such as phospholipids and fatty acids) form a spherical monolayer enclosing an aqueous interior [7–10]. These reverse micelle aerosols act as vehicles for atmospheric transport, affect radiative transfer and the earth's climate [8,11], and may have provided an environment conducive for prebiotic chemical reactions [12,13].

An interesting question is whether the reverse micellar structure could survive *in vacuo*. Gas-phase aggregates of various surfactants [14–26] have been observed utilizing electrospray ionization (ESI) [27,28] mass spectrometry. Most of these experiments used surfactants which only tend to form direct micelles, i.e., the surfactants are oriented so that the alkyl chains constitute the core and the polar heads form the shell. To the best of our knowledge, there are only a few studies concerning spatially ordered surfactant assemblies which may be characterized by a reverse micellar structure, and here we summarize the relevant work. Sharon et al. [22] obtained ESI mass spectra of multiply charged cetyltrimethylammonium bromide (CTAB) aggregates from CTAB reverse micellar solutions, and found no exchange of bromide ions from the surfactant headgroups with acetate ions present in the bulk solvent. They concluded that the orientation of surfactants in reverse micelles could be preserved *in vacuo*, and for reverse micelles encapsulating proteins, the interactions between surfactants and the encapsulated protein remain during the phase transition. Thereafter, Wang et al. [29] presented molecular dynamics simulations of the same system *in vacuo*. They found that the reverse micelles remained stable throughout the simulation with the polar headgroups facing inward and the apolar tails facing the vacuum. They also found

* Corresponding author. Tel.: +1 718 997 3271; fax: +1 718 997 5531.
E-mail address: Jianbo.liu@qc.cuny.edu (J. Liu).

1387-3806/$ – see front matter © 2010 Elsevier B.V. All rights reserved.
doi:10.1016/j.ijms.2010.03.005

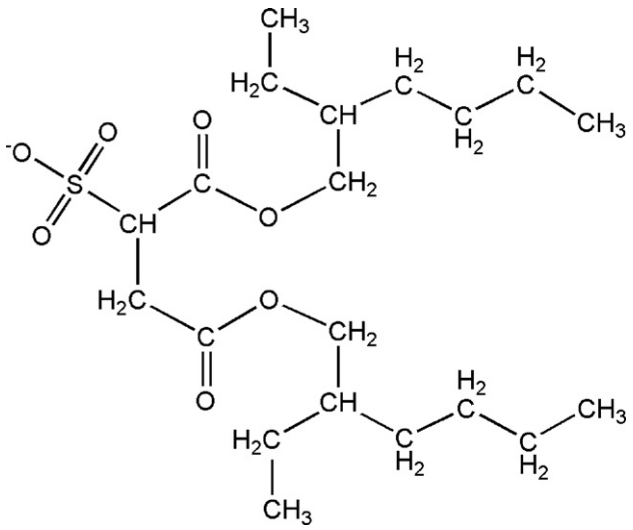

Fig. 1. Skeletal formula of bis(2-ethylhexyl) sulfosuccinate anion (AOT).

that direct CTAB micelles invert into reverse micelles when they are dehydrated in a vacuum. Another surfactant molecule well suited to form stable reverse micelles in apolar solvents is sodium bis(2-ethylhexyl) sulfosuccinate (NaAOT), which has two branched alkyl chains as shown in Fig. 1. Bongiorno et al. [21] reported self-assembling of NaAOT in the gas phase using ESI and matrix-assisted laser desorption/ionization (MALDI) mass spectrometry. They used solutions below the critical micelle concentration (CMC) of NaAOT and observed singly charged aggregates. Noticing that similar mass spectra were obtained independent of the ionization method and solvent used, and that the NaAOT aggregation number was close to that in apolar media, they proposed that self-assembling of surfactants occurs during the evaporation step and that aggregates consist of a reverse micelle-like structure. More recently, Giorgi et al. [24,25] reported gas-phase NaAOT assemblies with counter ions, Na^+, partially or completely replaced by various alkaline metal ions, as well as aggregates carrying alkali salt.

In these experiments, formation of gas-phase aggregates, either by electrospray of a reverse micellar solution or via self-assembling of gas-phase surfactants, is associated with the solvent evaporation. Elimination of an apolar solvent weakens the driving force towards reverse micelle formation, but the electrostatic force between polar heads and their counter ions still exists. Molecular dynamics simulations demonstrate that the overall structure of the reverse micelle in the vacuum is similar to that in an apolar solvent, but the surfactant tails collapse on the outer surface to form a more compact structure [30,31]. Taken together, these results indicate that it is possible to generate reverse micelles in the gas phase with the capability of incorporating guest molecules. Unlike their counterparts in solution, gas-phase reverse micelles would not have inter-micelle exchange of solutes. Therefore, they can provide isolated, "stable" molecular reactors to probe the chemistry of single molecules confined in the micellar core or bound to the micellar interface, and allow us to take measurements which have to be performed in a vacuum (such as mass spectrometry and single-particle imaging [32]). It is worth noting that encapsulation of biomolecules into gas-phase micelles may protect non-covalent interactions between biomolecular subunits in the vacuum, enabling direct determination of the subunit stoichiometry and ligand-binding properties [23].

In the above cited NaAOT studies, the mass spectra were dominated by singly charged species, and no multiply charged aggregates were detected with any significant abundance. In this paper, we report a guided-ion beam tandem mass spectrometry study of gas-phase NaAOT aggregates. We show that multiply charged, large NaAOT reverse micelles can be generated in a vacuum, and amino acids can be encapsulated in the interior of gas-phase reverse micelles. This result demonstrates the application of NaAOT reverse micelles as nanometer-sized carriers of biomolecules in the gas phase. Furthermore, collision-induced dissociation (CID) of mass-selected reverse micelles with Xe was measured over a wide range of collision energies (E_{col}), allowing us to obtain insights into gas-phase reverse micellar structures and to evaluate the role played by the extra counter ions and encapsulated amino acids.

2. Experimental details

The guided-ion beam tandem mass spectrometer used in this study has been described in detail previously [33], along with the operation, calibration and data analysis procedures. Only a brief description is given here, emphasizing the unique features of this experiment. The apparatus consists of an ion source, a radio frequency (rf) hexapole ion guide [34], a quadrupole mass filter, a rf octopole ion guide surrounded by a scattering cell, a second quadrupole mass filter and a detector. Both quadrupole mass filters use Extrel 9.5 mm diameter tri-filter rods operating at 880 kHz (Extrel model 150 QC) to cover the mass/charge range from 1 to 4000. For conventional mass spectral measurements, the first quadrupole mass filter was operated in the rf-only mode as an ion guide, and mass scans were performed by the second quadrupole mass filter.

NaAOT reverse micelles were prepared in anhydrous hexane (Sigma–Aldrich, 95%) containing 2.0×10^{-3}, 5.0×10^{-3} and 10×10^{-3} M NaAOT ($C_{20}H_{37}NaO_7S$, molecular weight 444, Fluka, >99.0%, stored in a desiccator and used without additional purification), respectively. These concentrations are above the CMC of NaAOT in hexane (1.1×10^{-3} M) [35]. To verify the influence of pre-formed micelles in solution on gas-phase aggregates, another NaAOT solution was prepared at a concentration of 0.5×10^{-3} M, below the CMC. Water was added to the solution to achieve different water-to-AOT molar ratios ω_0, and the solution was sonicated for 10 min to create a transparent reverse micellar solution. The conductivity of the solution was measured using a YSI model 34 conductance meter. The micellar solution was sprayed into the ambient atmosphere through an electrospray needle using a syringe pump (KD Scientific model 100), at a constant flow rate of 0.04 ml/h. The electrospray needle was prepared from 35 gauge hypodermic stainless steel tubing (0.13 mm o.d. × 0.06 mm i.d., Small Parts Inc.), and biased at 3000 V relative to ground. Positively charged droplets formed from the electrospray needle were fed into a heated desolvation capillary. Initial radii of spray droplets are estimated to be ~0.6 μm [36–38]. Assuming solvent evaporates uniformly from the droplet surface, the time for hexane evaporation is estimated at less than 0.5 ms [39]. The distance between the electrospray needle tip and the sampling orifice of the capillary was ~1 cm. The capillary was biased at 70 V relative to ground and heated to 150 °C. Charged liquid droplets underwent desolvation as they passed through the heated capillary, converting to gas-phase ions. A skimmer with an orifice of 1.5 mm (Beam Dynamics, Inc.) was located 5 mm from the capillary end, separating the ion source chamber and the hexapole ion guide. The skimmer was biased at 10 V relative to ground, and the electrical field between the capillary and the skimmer removed remaining solvent molecules by collision-induced desolvation [40], and prevented large solvent clusters from depositing downstream [41,42]. Ions that emerged from the skimmer were passed into a rf hexapole ion guide at a pressure of 10 mTorr, leading to collisional focusing [43–45]. Ions

subsequently passed into a set of entrance focusing lenses followed by a quadrupole mass filter. Mass-selected ions were then injected into a rf octopole ion guide which trapped ions in the radial direction. The octopole ion guide operated at 2.6 MHz with a peak-to-peak amplitude of 700 V. DC bias voltage was applied to the ion guide, and its amplitude was varied from −500 to +500 V. The dc bias voltage was used in the retarding potential analysis (RPA) [46] to determine the initial kinetic energy of selected ions, i.e., intensities of ions were measured while sweeping the octopole bias. The dc bias voltage also allowed control of the kinetic energy of ions in the laboratory frame. Ion kinetic energies in the lab frame (E_{lab}) are converted to collision energies in the center-of-mass frame (E_{col}) using $E_{col} = E_{lab} \times m_{neutral}/(M_{ion} + m_{neutral})$, where $m_{neutral}$ and M_{ion} are masses of neutral collision gas and ions, respectively. The octopole passed through a scattering cell containing the collision gas Xe (Spectral Gases, 99.995%) at ~0.01 mTorr. The scattering cell pressure was measured by a capacitance manometer (MKS Baratron 690 head and 670 signal conditioner). Precursor ions and their fragment ions were collected by the octopole ion guide, and directed to the second mass spectrometer for mass analysis. Ion signals were counted using a pulse-counting electron multiplier.

One issue for CID of reverse micellar ions concerns their size. Assuming gas-phase reverse micelles are spherical, a micelle made of 20 NaAOT molecules has a radius of ~19 Å. The collision cross-section of this micelle with Xe is estimated to be 1300 Å^2. To keep multiple collision effects to an insignificant level, the pressure of Xe in the scattering cell was maintained at 0.01–0.013 mTorr during CID cross-section measurements. In this range of pressure, the probability of a single collision between a micellar ion and Xe is ~15%, and of double collisions is <4%. The majority of micellar ions (> 81%) passed through the scattering cell without interacting with Xe at all. We note that in previously reported CID experiments of both direct [14,22,23] and reverse [21,22,24,25] micellar ions, Ar or He was used as a collision gas and the collision gas pressure was increased to a relatively high value to achieve high dissociation yields. Under such conditions, multiple collisions were prevailing, and primary fragment ions underwent further dissociation. As a consequence, the dissociation product ion mass spectra were dominated by small fragment ions, and the "stated" collision energies (often indicated in the lab frame) did not reflect the energy dependence of dissociation.

CID of multiply charged ions results in numerous dissociation channels and product ions of varying mass and charge. It is difficult to measure cross-sections for individual channels. First, because of the low Xe pressure, intensities of product ions were too low to achieve a good signal-to-noise ratio. Secondly, because CID of multiply charged precursor ions accompanies charge separation [37,47,48], some product ions possess mass/charge that is beyond the mass spectrometer detection limit (i.e., 4000). Finally, for the given octopole rf frequency (f) and amplitude (V_{rf}), only ions with radial velocities up to well-defined cutoff values can be confined by the octopole [34]. At high E_{col}, light product ions may have high radial velocities. In order for these ions to have stable trajectories, the rf frequency should be large enough that the field changes polarity frequently on the time scale of the ions' radial motion in the octopole. On the other hand, the magnitude of the effective potential (U_{eff}) confining the ions' radial motion is proportional to V_{rf}/mf^2. High frequency dictates high V_{rf}, however, there are V_{rf} limits set by arcing, and high V_{rf} also tends to exacerbate the breakdown of adiabaticity [34]. For the mass ratios in this system, it is difficult to avoid loss of some product ions at high E_{col}. For these reasons, we did not report cross-sections for individual channels. Total CID cross-section at each E_{col} was measured based on the loss of precursor ions, the target gas pressure, and the calibrated effective length of the scattering cell [33]. To allow subtraction of background from the detector, and from dissociation occurring in the ion guide portions outside the scattering cell, precursor ions were measured with the Xe gas directed into the scattering cell ("cell-on") and with the same flow directed into the vacuum chamber ("cell-off"). Since these two conditions only differ in the gas density in the scattering cell, the difference in "cell-off" and "cell-on" provides an accurate count of CID inside the cell.

Because the ion intensities measured were low, it is important to minimize systematic variation in experimental conditions that might be caused by drifting potentials, change in ion beam intensities, etc. In experiments, we cycled through different E_{col} several times. RPA measurements of precursor ions were performed before and after each experiment to check the initial kinetic energy of the primary ion beam. The entire experiment was repeated several times to check the reproducibility. Based on the reproducibility of the measurements, we estimated that the relative error of CID cross-sections (e.g., uncertainty in comparing data for different E_{col}) is ~20%.

3. Results

3.1. Mass spectra of NaAOT/water/hexane reverse micellar solutions

Mass spectra obtained by ESI of NaAOT (5.0×10^{-3} M)/water/hexane reverse micellar solutions with varying values of ω_0 are depicted in Fig. 2. It was found that, within the instrument detection range (mass/charge = 1–4000), gas-phase aggregates have the composition of $[(NaAOT)_nNa_z]^{z+}$. Each aggregate hosts extra Na^+ ions (in addition to AOT counter ions), which account for its overall charge. Assignments of mass peaks are based on their aggregation numbers (n) and charges (z), and the labels for the same charge states are grouped together. For convenience, in the following discussion the aggregates are indicated as n/z. The most intense mass peaks in Fig. 2a and b have been attributed to the singly charged species, of which 5/1 and 6/1 are the strongest, and the relative abundance of aggregates decreases with increasing aggregate size and charge. A series attributed to singly charged $[(NaAOT)_nH]^+$ have been identified in Fig. 2a and b, of which one Na^+ is substituted for a proton. But the intensities of $[(NaAOT)_nH]^+$ are much lower compared to corresponding $[(NaAOT)_nNa]^+$.

As demonstrated in Fig. 2a and b, the distributions of gas-phase NaAOT aggregate size, and therefore charge, are strongly dependent on the values of ω_0, and heavier aggregates form upon increasing ω_0. At ω_0 = 0–5 (mass spectrum for ω_0 = 5 not shown, but similar to ω_0 = 0), the maximum aggregation number (n_{max}) and charge (z_{max}) are 26 and 3, respectively. The values of n_{max} and z_{max} increase to 35 and 4 at ω_0 = 6.5 (not shown), and to 44 and 5 at ω_0 = 10. The actual values of n_{max} could be larger, since the maximum size at each ω_0 is approaching the detection limit of the mass filter. There is a minimal aggregation number (n_{min}) for each charge state 2, 4, 8, 14 and 20 for z = 1, 2, 3, 4 and 5 respectively. Increasing ω_0 from 10 to 20 does not change the size and charge distribution of gas-phase aggregates. But the abundance of multiply charged species relative to that of singly charged species increases markedly as ω_0 is progressively increased. When ω_0 exceeds 20, the mass spectra become congested and poorly resolved. The mass spectrum of ω_0 = 30 is shown in Fig. 2c, with a progressively growing background signal starting at mass/charge = 1500. A reasonable explanation for the broadened and diffused spectrum at ω_0 = 30 is that the abundance of large, multiply charged micelles increases at high ω_0, and higher charge states are more susceptible to in-source dissociation with residual gas because they have higher collision energies than low charge states at the same acceleration voltage [49]. Another possible contribution to the complexity of mass spec-

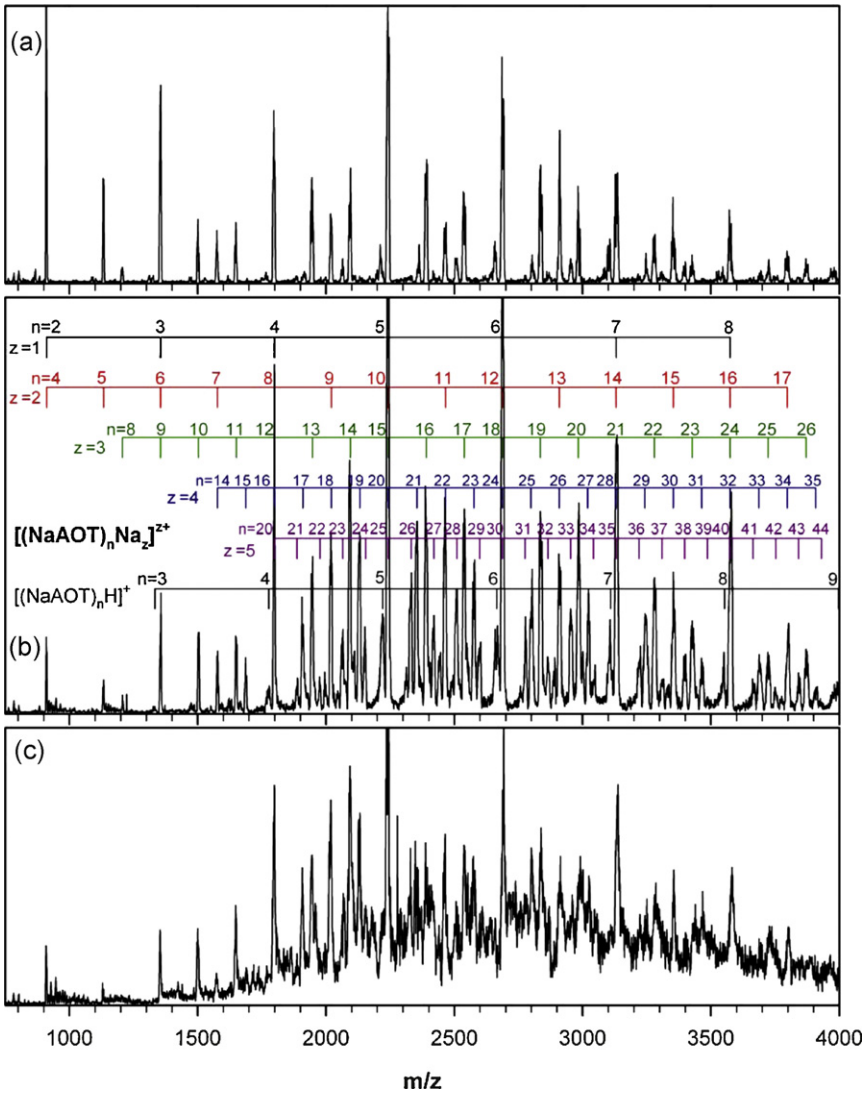

Fig. 2. ESI mass spectra of NaAOT (5.0×10^{-3} M)/water/hexane reverse micellar solutions with different water-to-AOT ratios ω_0. (a) $\omega_0 = 0$, (b) $\omega_0 = 10$ and (c) $\omega_0 = 30$.

tra at extremely high water loading could be attributed to residual water molecules within reverse micelles. Because gas-phase aggregates underwent collisions with air and solvent molecules, portions of small aggregates observed in Fig. 2a–c could be yielded from dissociation of large aggregates by sequential losses of AOT and Na^+.

We also varied the NaAOT concentration in hexane while keeping the value of ω_0 at 10. For solutions containing 2.0×10^{-3}, 5.0×10^{-3} and 10×10^{-3} M NaAOT (all above the CMC), we found no difference in the distributions of aggregate size and charge, with $n_{max} = 44$ and $z_{max} = 5$ for these solutions. In other words, above the CMC with fixed water content, the NaAOT concentration does not affect gas-phase aggregates. However, for a solution of 0.5×10^{-3} NaAOT (below the CMC), n_{max} and z_{max} decrease to 26 and 3, respectively.

The dependence of observed n_{max} on NaAOT concentration and ω_0 for gas-phase aggregates is analogous to that for the micellar solution. Above the CMC, the reverse micelle size is determined by the water content. Dry NaAOT reverse micelles in apolar solvents have an average aggregation number around 20 [31,50,51]. Aggregation numbers of wet reverse micelles could be estimated using $n = 4\pi r_{core}^2/A_{head}$ and $r_{core} = 1.7\ \omega_0$(Å) [52], where r_{core} is the radius of the micellar core and A_{head} is the area occupied by each AOT polar head at the interface (0.52 nm^2) [1,53,54]. Typical values of n in solution are estimated to be 18, 32 and 70 for $\omega_0 = 5$, 6.5 and 10, respectively. The values of observed gas-phase n_{max}, except for $\omega_0 = 10$, are comparable to the corresponding n in solution. We could not rule out the possibility of missing large gas-phase aggregates at mass/charge >4000, since theoretical simulations suggest that gas-phase micelles could have more compact structures compared to those in solution [30]. However, the large aggregates would be less likely in high abundance judging from the ion intensity profiles observed in these mass spectra. In summary, the correlation between the size of gas-phase aggregates and ω_0 of starting solution – a key property of reverse micelles in solution, implies that gas-phase aggregates retain a memory of starting solution. This is consistent with the fact that under certain conditions ESI can preserve non-covalent interactions in large macromolecular complexes [16,18,20].

3.2. Mass spectra of NaAOT monomers in methanol/water (1:1)

To further investigate the effects of solution conditions on the size and charge distribution of gas-phase aggregates, we carried out a control experiment under the same conditions except

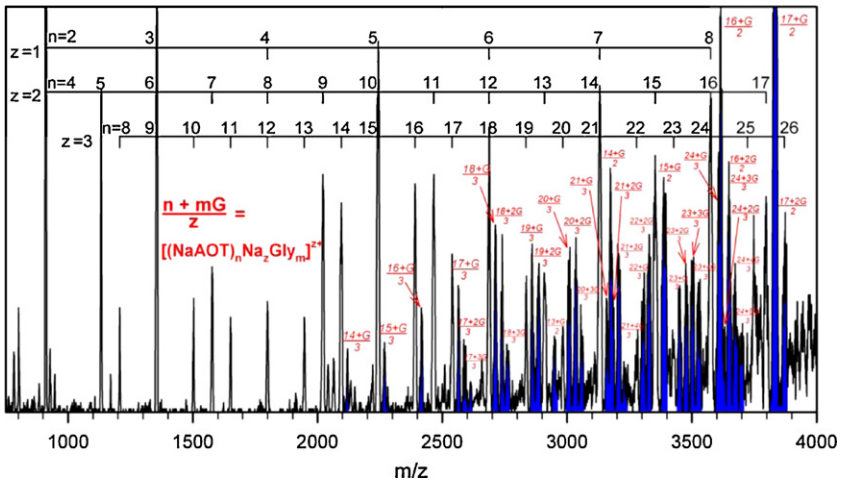

Fig. 3. ESI mass spectrum of a reverse micellar solution containing 5.0×10^{-3} M NaAOT, 5.0×10^{-2} M H_2O ($\omega_0 = 10$) and 1.0×10^{-3} M glycine in hexane.

that we used a methanol/water (1:1 volume ratio) solution of 1.0×10^{-3} M NaAOT (below the CMC in water, 2.0×10^{-3} M [35]). In this case, only aggregates of $n = 2$–26 and $z = 1$–3 were observed, which is similar to the spectrum obtained from a dry NaAOT/hexane micellar solution (i.e., $\omega_0 = 0$) or a NaAOT (0.5×10^{-3} M)/water ($\omega_0 = 10$)/hexane solution. In addition, the distribution of size and charge is independent of NaAOT concentration in methanol/water, in the range of 0.7×10^{-3}–5.0×10^{-3} M which was chosen to bracket the CMC.

Our ESI mass spectra of NaAOT in methanol/water are somewhat different than those reported by Bongiorno et al. and Giorgi et al. [21,24,25]. Although the NaAOT solution was prepared in a similar manner, their ESI mass spectra are dominated by $[(NaAOT)_nNa]^+$, and doubly and triply charged species are of negligible abundance. Discrepancy is also noted in the shape of ion abundance profiles. In our mass spectra aggregates 5/1 and 6/1 exhibit the highest abundance, while in their mass spectra the trimeric species 3/1 is the base peak. These discrepancies are most likely related to the differences in the ESI conditions and instrumentation. In their experiments, ESI was operated at a flow rate of 0.12–4.2 ml/h with a nitrogen sheath gas. The capillary was heated to 230 °C, and mass spectra were measured on an ion-trap mass spectrometer. Our ESI source was operated at a lower flow rate (0.04 ml/h) and with no sheath gas. We maintained the capillary temperature at 150 °C, and collected spectra on a quadrupole mass spectrometer. Some of these different operating conditions may exert counteracting effects on size and charge distributions. For example, the sheath gas and high capillary temperature increased the evaporation rate and reduced the time available for desorption of ions during stages of low droplet charge density, which may lead to low intensities of lower charge states [49]. On the other hand, a high flow rate in ESI increased the evaporation time and favored lower charge states. We also found that multiply charged aggregates are sensitive to the potential between the capillary and the skimmer, because they gain higher translational energies than the lower charge states in the same electrical field. In our experiment, the skimmer was biased at 10 V. Aggregates of $z \geq 3$ achieved the highest intensity at capillary voltage of 70 V, but completely disappeared when the capillary voltage increased to more than 110 V. Therefore, the absence of high charge states in previous reports may be due to the significant in-source CID. This comparison implies that ESI and instrumental conditions are another important controlling factor for the distribution of gas-phase aggregates. For this reason, all data in this paper were collected under the same experimental conditions unless otherwise stated, so that we can focus on effects of solution conditions.

3.3. Mass spectrum of NaAOT reverse micelles encapsulating glycine

In this experiment, we prepared NaAOT reverse micelles in hexane with $\omega_0 = 10$, into which glycine (Gly) was added ([NaAOT] = 5.0×10^{-3} M and [Gly] = 1.0×10^{-3} M). Reverse micelles were then electrosprayed to the gas phase, followed by mass analysis. We chose a simple amino acid in order to facilitate the identification of key factors in gas-phase reverse micelle encapsulation.

The mass spectrum of Gly-encapsulating NaAOT reverse micelles is shown in Fig. 3. In the mass/charge range below 2000, mass spectrum of reverse micelles with Gly incorporated is indistinguishable from that of empty reverse micelles shown in Fig. 2b, implying that at this mass/charge range, gas-phase aggregates are unoccupied. Occupied NaAOT aggregates are observed with compositions of $[(NaAOT)_nNa_zGly_m]^{z+}$ in the mass/charge range above 2000. These species become prevailing at mass/charge above 3000. In the figure, we indicate these species in blue shaded areas, and label them as $(n + mG)/z$. We note that, although Na^+ and/or H^+ can be attached to Gly molecule [55,56], no monomers and clusters of sodiated or protonated Gly have been detected, indicating that all Gly molecules are confined within NaAOT aggregates.

There is a strong correlation between the encapsulation capability and the size of gas-phase NaAOT aggregates. No encapsulation was detected for aggregates with an aggregation number less than 13. Aggregates of $n \geq 13$ can entrap one Gly molecule, while those of $n \geq 16$ can entrap two. Up to three Gly molecules can be accommodated in single aggregates of $n \geq 17$, four Gly molecules in those of $n \geq 21$, and five in those of $n \geq 24$. Assuming a spherical reverse micelle-like geometry for NaAOT aggregates, its core diameter D is roughly equal to $\sqrt{n \times A_{head}/\pi}$ where A_{head} is the area of the AOT polar head as defined above. D is calculated to be 1.4, 1.6, 1.7, 1.9 and 2.1 nm for $n = 13$, 16, 17, 21 and 25, respectively. The size of a Gly molecule is 0.6–0.7 nm. Therefore, the maximum number of encapsulated Gly molecules roughly matches the micellar core size. Among Gly-encapsulating aggregates, $(17+G)/2$ displays the highest abundance, indicating a particularly stable geometric structure for this assembly.

There is a weak charge dependence of Gly encapsulation. For example, for occupied aggregates of the same size, doubly charged species have a higher abundance than triply charged ones (e.g., $(15+G)/2$ vs. $(15+G)/3$ and $(17+G)/2$ vs. $(17+G)/3$), and doubly charged species can entrap more Gly molecules (e.g., $(16+G)/2$ vs. $(16+G)/3$). We also note that upon encapsulation of Gly the intensities of highly charged micelles (i.e., $z > 3$) dramatically decreases,

implying that Gly and Na^+ compete for surfactants, and AOT may have a higher affinity for Gly than for Na^+.

These observations deviate from expectations if random associations are assumed between surfactants and Gly molecules. We also performed ESI experiments with arginine, aspartic acid, histidine, proline, tryptophan or tyrosine incorporated into NaAOT reverse micelles, and found a similar dependence of encapsulation on micelle size. (The analyses of these amino acid-encapsulating NaAOT reverse micelles will be reported in a separate paper). These findings strongly support a reverse micelle-like structure for gas-phase NaAOT aggregates containing biomolecules in their interior. To emphasize the fact that we are dealing with spatially ordered reverse micelle-like NaAOT aggregates, we will refer to these aggregates as gas-phase reverse micelles (or micellar ions) in the remainder of the discussion.

3.4. CID of gas-phase NaAOT reverse micelles

3.4.1. Empty reverse micelles

One issue in interpreting CID of NaAOT reverse micellar ions is that there are mass coincidences among different charge states. Intensities of peaks corresponding to singly charged micellar ions include the shares of all multiply charged ions at the same mass/charge positions. For example, mass/charge of 2687 represents at least four overlapping charge states, 6/1, 12/2, 18/3 and 24/4. For this reason, we chose, in ascending order of micelle size and charge, 13/2, 15/2, 17/2, 16/3, 17/3, 19/3 and 20/3 as precursor ions. Selection of these ions circumvents the complication of mass coincidence with other charge states, and simplifies the interpretation of product ion spectra. Consequently, the dissociation behavior of each micellar ion is clearly revealed. Fig. 4 shows the product ion mass spectra from CID of mass-selected micellar ions. To map out all dissociation product ions within the instrument mass/charge detection limit, data in Figs. 4 and 6 were obtained at a relatively high Xe pressure (0.15 mTorr) in the scattering cell. Because of multiple collisions between precursor ions and Xe at a high gas pressure (and primary fragment ions may continue to undergo collisions that cause them to fragment as well), the relative intensities of product ions in Fig. 4 do not reflect the branching ratio. However, all product ions in Fig. 4 were observed under single-collision conditions as well.

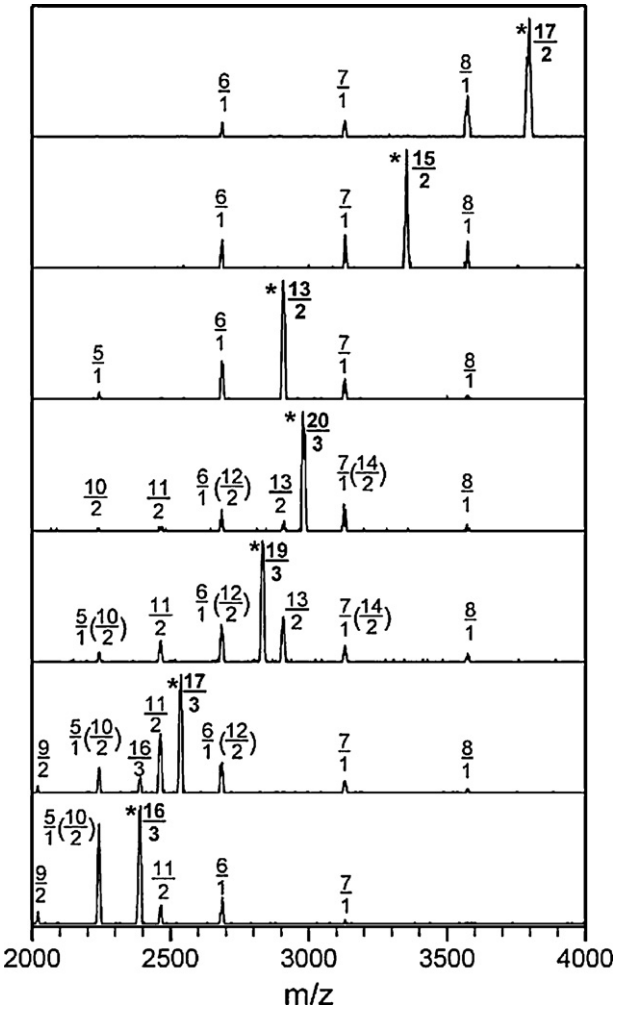

Fig. 4. CID mass spectra of mass-selected NaAOT reverse micellar ions. Spectra were measured at E_{col} = 1.0 eV for doubly charged ions and E_{col} = 1.5 eV for triply charged ions, with a 0.15 mTorr Xe in the scattering cell. Ions are labeled as $\frac{n}{z}$ Asterisks indicate precursor ions, and the labels in parentheses are alternative assignments for product ions.

Table 1 summarizes dissociation channels for individual precursor ions. Unless otherwise stated, both complementary product ions, produced from a dissociation leading to two charged products, were observed in mass spectra and are included in the Table. Bongiorno et al. [21] and Giorgi et al. [24] reported CID of singly charged $[(NaAOT)_nNa]^+$ precursor ions, in which losses of neutral NaAOT units are the preferred fragmentation paths. For multiply charged micellar ions, dissociation of reverse micelles strongly depends on their charge states. For doubly charged micellar ions, CID exclusively produces singly charged products. It is interesting to note that the major CID channels for doubly charged micellar ions correspond to divisions of precursor ions into two nearly equally-sized products, e.g., 15/2 → 8/1 + 7/1. CID of triply charged micellar ions becomes more complex, and products include both singly and dou-

Table 1
CID products of gas-phase NaAOT reverse micellar ions.

Precursor ions[a]	Dissociation channels	Precursor ions[a]	Dissociation channels
$\frac{13}{2}$	$\frac{8}{1}+\frac{5}{1}$	$\frac{16}{3}$	$\frac{11}{2}+\frac{5}{1}$
	$\frac{7}{1}+\frac{6}{1}$		$\frac{10}{2}+\frac{6}{1}$
			$\frac{9}{2}+\frac{7}{1}$
$\frac{15}{2}$	$\frac{9}{1}+\frac{6}{1}$[b]	$\frac{17}{3}$	$\frac{16}{3}+1$
	$\frac{8}{1}+\frac{7}{1}$		$\frac{12}{2}+\frac{5}{1}$
			$\frac{11}{2}+\frac{6}{1}$
			$\frac{10}{2}+\frac{7}{1}$
			$\frac{9}{2}+\frac{8}{1}$
$\frac{17}{2}$	$\frac{11}{1}+\frac{6}{1}$[b]	$\frac{19}{3}$	$\frac{13}{2}+\frac{6}{1}$
	$\frac{10}{1}+\frac{7}{1}$[b]		$\frac{14}{2}+\frac{5}{1}$
	$\frac{9}{1}+\frac{8}{1}$[b]		$\frac{12}{2}+\frac{7}{1}$
			$\frac{11}{2}+\frac{8}{1}$
			$\frac{10}{2}+\frac{9}{1}$[b]
		$\frac{20}{3}$	$\frac{14}{2}+\frac{6}{1}$
			$\frac{13}{2}+\frac{7}{1}$
			$\frac{12}{2}+\frac{8}{1}$
			$\frac{11}{2}+\frac{9}{1}$[b]
			$\frac{10}{2}+\frac{10}{1}$[b]

[a] The precursor and product ions are indicated as $\frac{n}{z}$ where n is the aggregation number and z is the charge.

[b] $\frac{9}{1}$, $\frac{10}{1}$ *and* $\frac{11}{1}$ are beyond the mass/charge detection limit of the mass spectrometer.

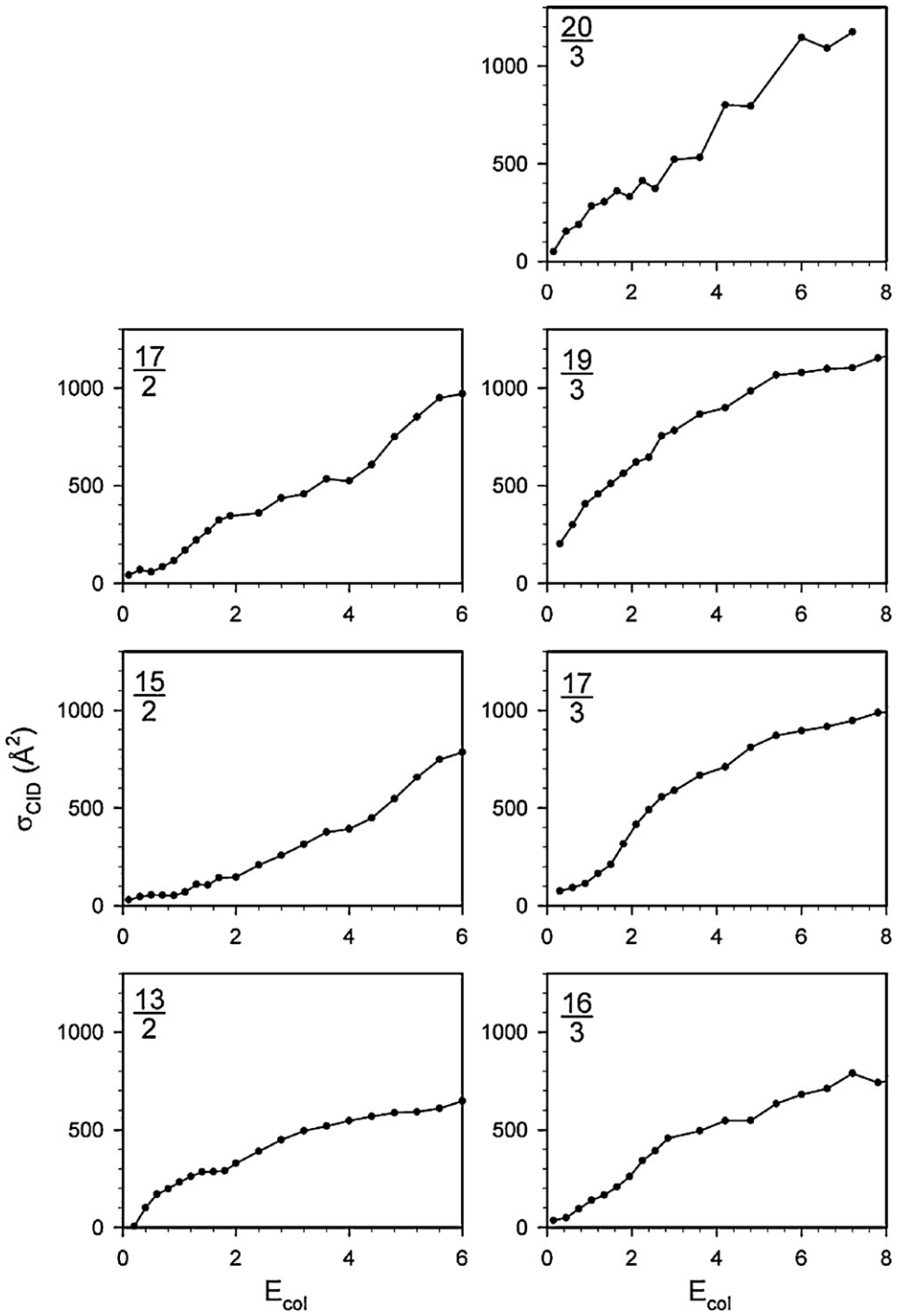

Fig. 5. CID cross-sections of mass-selected NaAOT reverse micellar ions (labeled as $\frac{n}{z}$), measured under single-collision conditions.

bly charged ions, as well as small amounts of triply charged ions. Because of overlapping of singly, doubly and triply charged ions, some peaks may actually be attributed to more than one product ion mass. We indicate alternative assignments using parentheses for some product ions in Fig. 4. It is also possible to produce three singly charged products from CID of triply charged precursor ions; however, these channels cannot be assigned unambiguously and thus are not included in the table.

We report total CID cross-sections (σ_{CID}) for precursor ions in Fig. 5, in the E_{col} range of 0.1–6.0 eV for doubly charged ions and 0.1–8.0 eV for triply charged ions. All collision energies are given in the center-of-mass frame. The main points of cross-section measurements are as follows: (1) σ_{CID} shows threshold-like behavior at low E_{col} and increases as E_{col} rises. (2) σ_{CID} strongly depends on reverse micelle size. At E_{col} = 6.0 eV, σ_{CID} increases from ~600 Å^2 for 13/2 to ~950 Å^2 for 17/3 and ~1150 Å^2 for 20/3. (3) σ_{CID} is enhanced by the micelle charge. For example, 17/3 has larger σ_{CID} than 17/2 at all collision energies. (4) We compared σ_{CID} of large micellar ions with their hard-sphere collision cross-sections ($\sigma_{hard\text{-}sphere}$) with Xe. At our highest E_{col}, σ_{CID} for 17/3, 19/3, and 20/3 are 1000–1200 Å^2. Assuming spherical geometries for reverse micellar ions, their hard-sphere collision cross-sections are 1200–1300 Å^2. σ_{CID} is approaching the collision limit at our highest E_{col}. Therefore, at sufficiently high energies, we expect that nearly every

hard-sphere collision leads to dissociation, and σ_{CID} becomes independent of E_{col} [57]. For micellar ions of $n < 17$, maximum σ_{CID} are smaller than their $\sigma_{hard\text{-}sphere}$. However, it is possible that they have not reached the plateau in close proximity to $\sigma_{hard\text{-}sphere}$ at our highest E_{col}. In any case, σ_{CID} provides a measure of the lowest limit of the average micelle size.

3.4.2. Gly-encapsulating reverse micellar ions

It is interesting to compare CID of empty and Gly-encapsulating reverse micellar ions, because CID of occupied reverse micelles may involve a competition between stripping surfactants and expelling confined amino acids. Such competition should be driven by the precursor ion structure, and by the stability of neutral and charged products formed. To enable a direct comparison, CID of Gly-encapsulating reverse micellar ions were performed using similar aggregation numbers and charges as those employed for empty micellar ions, i.e., $(13+G)/2$, $(15+G)/2$, $(17+G)/2$, $(16+G)/3$, $(17+G)/3$, $(19+G)/3$ and $(20+G)/3$.

Fig. 6 shows mass spectra of CID product ions for mass-selected reverse micellar ions incorporating Gly, and Table 2 summarizes their dissociation channels. Occupied reverse micellar ions have distinct dissociation channels from the corresponding empty ones.

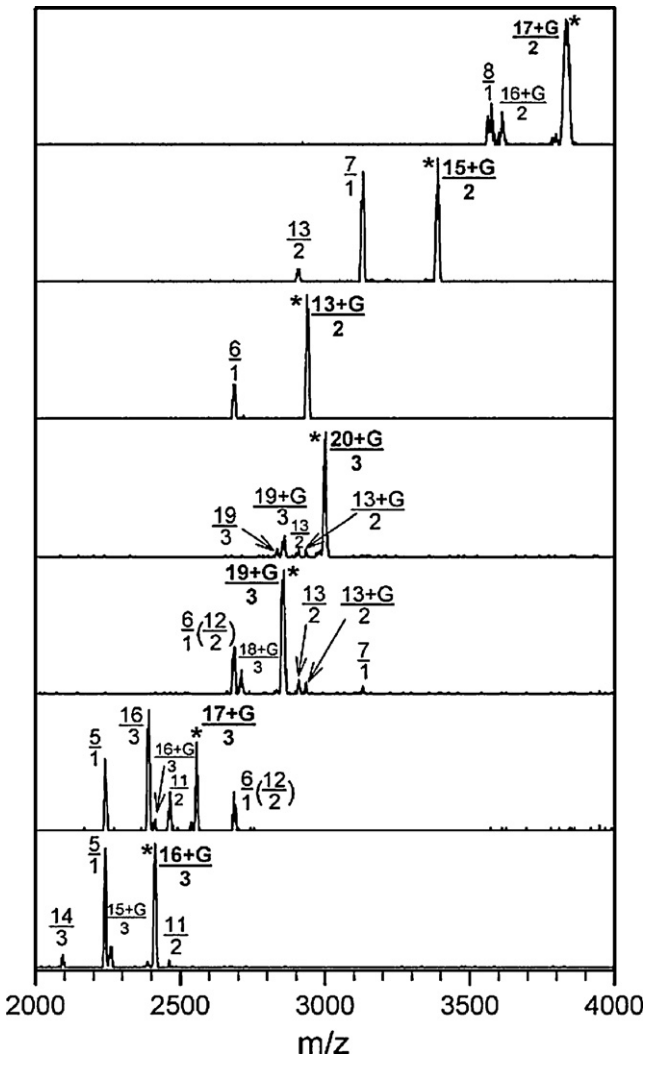

Fig. 6. CID mass spectra of mass-selected NaAOT reverse micellar ions encapsulating Gly. Spectra were measured at E_{col} = 1.0 eV for doubly charged ions and E_{col} = 1.5 eV for triply charged ions, with a 0.15 mTorr Xe in the scattering cell. Ions are labeled as $\frac{n+mG}{z}$ and $\frac{n}{z}$. Asterisks indicate precursor ions, and the labels in parentheses are alternative assignments for product ions.

Table 2
CID products of gas-phase NaAOT reverse micellar ions encapsulating Gly.

Precursor ions[a]	Dissociation channels	Precursor ions[a]	Dissociation channels
$\frac{13+G}{2}$	$\frac{7}{1}$(not detected) + $\frac{6}{1}+G$	$\frac{16+G}{3}$	$\frac{15+G}{3}+1$
			$\frac{14}{3}+2+G$
			$\frac{11}{2}+\frac{5}{1}+G$
$\frac{15+G}{2}$	$\frac{13}{2}+2+G$	$\frac{17+G}{3}$	$\frac{16+G}{3}+1$
	$\frac{8}{1}$(not detected) + $\frac{7}{1}+G$		$\frac{16}{3}+1+G$
			$\frac{12}{2}+\frac{5}{1}+G$
			$\frac{11}{2}+\frac{6}{1}+G$
$\frac{17+G}{2}$	$\frac{16+G}{2}+1$	$\frac{19+G}{3}$	$\frac{18+G}{3}+1$
	$\frac{8}{1}+\frac{9}{1}+G$[b]		$\frac{13+G}{2}+\frac{6}{1}$
			$\frac{13}{2}+\frac{6}{1}+G$
			$\frac{12}{2}+\frac{7}{1}+G$
		$\frac{20+G}{3}$	$\frac{19+G}{3}+1$
			$\frac{19}{3}+1+G$
			$\frac{13+G}{2}+\frac{7}{1}$
			$\frac{13}{2}+\frac{7}{1}+G$

[a] The precursor and product ions are indicated as $\frac{n+mG}{z}$ and $\frac{n}{z}$, where n is the aggregation number, z is the charge and m is the number of encapsulated glycine molecules.
[b] $\frac{9}{1}$ is beyond the mass/charge detection limit of the mass spectrometer.

As listed in Table 2, dissociation of occupied reverse micelles produces large product ions, some of which still encapsulate Gly, suggesting that encapsulation of Gly may improve the overall stability of reverse micellar structures. The smallest stripped micellar ion still capable of hosting a Gly molecule is $(13+G)/2$, similar to what we observed in the mass spectrum of Gly-encapsulating reverse micelles (Fig. 3). Fig. 6 also shows that, under the same conditions, $(17+G)/2$ yields less dissociation than other precursor ions. It follows that $(17+G)/2$ has higher stability, again in agreement with ESI mass spectral results. σ_{CID} for Gly-encapsulating reverse micellar ions are shown in Fig. 7. Generally, occupied micellar ions have similar or slightly higher σ_{CID} than empty micellar ions. Consistent with its high stability, $(17+G)/2$ has a smaller σ_{CID} than all other precursor ions except $(13+G)/2$.

4. Discussion

4.1. Dependence of gas-phase reverse micelle size and charge on solution conditions

Interpretation of the effects of solution conditions hinges on an understanding of the reverse micelle formation mechanism in the ESI process. The charge state of ions is related to the charge density at the droplet surface [49]. Initial radius (R) and charge (q) of the droplets produced by electrospray can be estimated as [36–38]:

$$R = \left(\frac{V_f \varepsilon}{K}\right)^{1/3} \quad (1)$$

$$q = 0.7[8\pi(\varepsilon_0 \gamma R^3)^{1/2}] \quad (2)$$

where ε and ε_0 are the permittivity of the solvent and the vacuum, respectively, γ is the surface tension of the solvent and K is the conductivity of the solution. According to these relationships, droplet radius and charge are

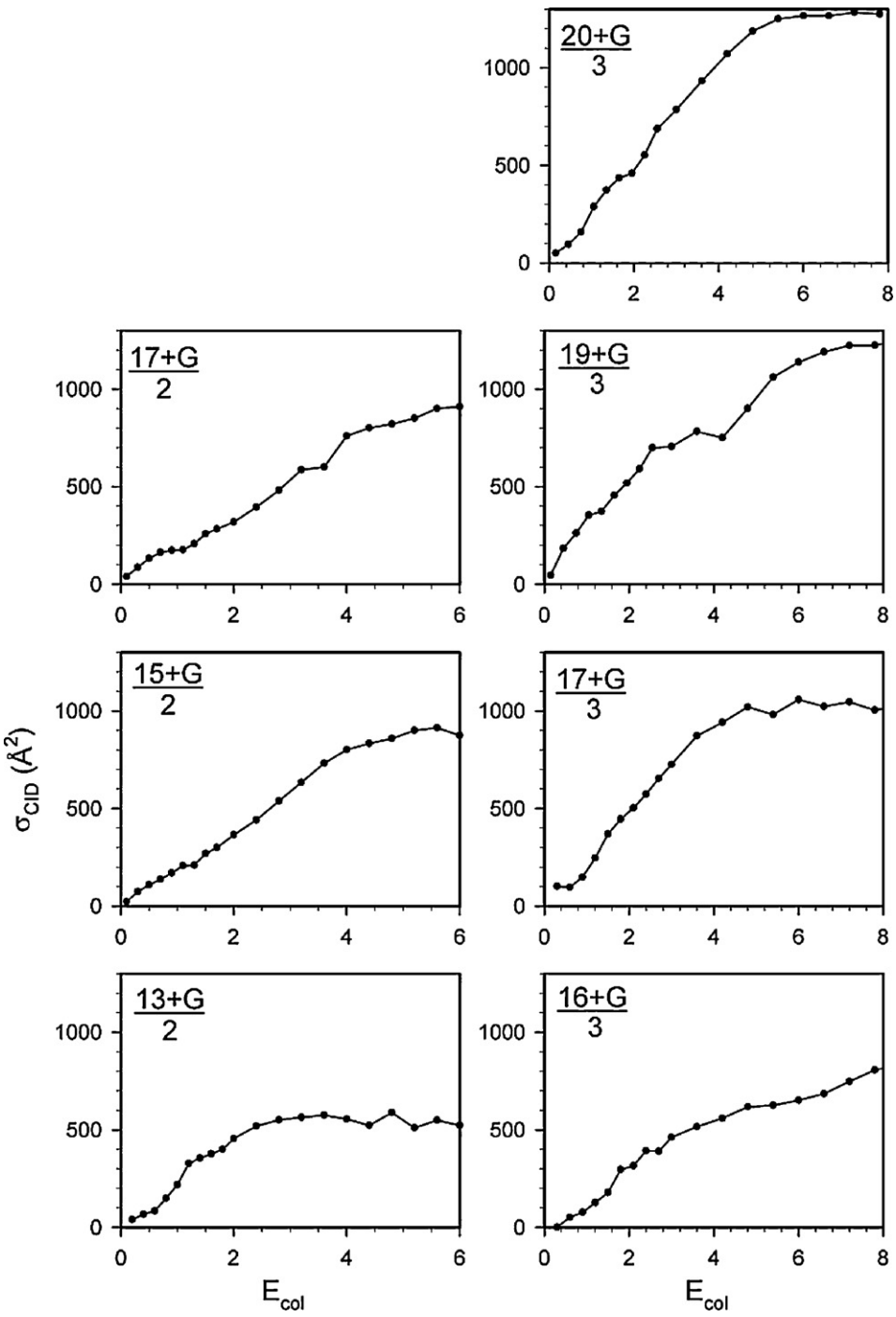

Fig. 7. CID cross-sections of mass-selected NaAOT reverse micellar ions encapsulating Gly (labeled as $\frac{n+mG}{z}$), measured under single-collision conditions.

predicted to be 0.59–0.62 μm and $2.1–2.2 \times 10^4$ for NaAOT ($0.5–5.0 \times 10^{-3}$ M)/water ($\omega_0 = 10$)/hexane, 0.92 μm and 5.4×10^4 for NaAOT (1.0×10^{-3} M) in methanol/water, and 0.6 μm and 2.8×10^4 for NaAOT (5.0×10^{-3} M) in methanol/water. Based on the predicted values of R and q, we found that neither the solvent nor the NaAOT concentration itself changes the charge density at droplet surface to a significant extent. Therefore, it is less likely that the charge density at droplet surface is responsible for formation of highly charged micellar ions (i.e., $z > 3$). Different charge distributions from different solutions must be related to the aggregate structures in solution.

One critical aspect of our experiment is whether large reverse micelles exist in the starting solution or not. For NaAOT/water/hexane solutions above the CMC, surfactants aggregate to form reverse micelles. When transferred from solution to the gas phase, reverse micelles may be able to preserve their structures, at least to some extent. In contrast, NaAOT cannot form micelles below the CMC. Neither can NaAOT form large micelles in anhydrous hexane or methanol/water. Consequently, in the latter three cases, self-assembling of NaAOT into large reverse micelles has to take place in the gas phase between electrospray and exposure to a high vacuum. The small size of gas-phase reverse micelles generated in these cases may be tentatively attributed to the fact that surfactants have a low concentration in the vapor state. Bongiorno et al. concluded a similar formation mechanism for methanol/water solution [21]. In sum, we adopted two

approaches for producing gas-phase reverse micelles, one utilizes NaAOT/water/hexane micellar solutions, and the other uses hexane or methanol/water solutions of monomeric NaAOT. While both cases may involve self-assembling of NaAOT in the gas phase, the micellar solution certainly helps formation of large gas phase aggregates. CID of the same micellar ions prepared with different approaches resulted in similar product ions, suggesting that the micellar structures are independent of the approach used for preparation.

It may be argued that multiply charged aggregates are not stable in a reverse micelle-like structure, because the micellar core has to host extra counter ions, and there is coulombic repulsion when the charges are too close to each other inside the core [21]. However, based on direct optimization of dry, isolated NaAOT reverse micelles [31], and molecular dynamics simulations of low ω_0 NaAOT reverse micelles in isooctane [58,59], most Na^+ ions penetrate the layer of AOT polar heads where the Na^+ ions coordinate with the sulfonate group. Some Na^+ can exist outside, where they coordinate with the carbonyl group of AOT [59]. We performed Mulliken charge analysis of AOT anion at the B3LYP/6-31 + $G(d,p)$ level of theory using Gaussian 03 [60]. Each sulfonate oxygen atom has a Mulliken charge close to or exceeding −0.6, and each carbonyl oxygen atom has a Mulliken charge close to −0.5. Na^+ may be able to interact with sulfonate and/or carbonyl oxygen atoms belonging to different AOT [21]. Therefore, from the point of view of electrostatic interactions, coordination of Na^+ with these oxygen atoms offers favorable structures for multiply charged reverse micelles, and could become one of important forces controlling aggregation. It is conceivable that for large reverse micelles, one single extra Na^+ is unable to interact with all AOT. Therefore, to stabilize the micellar structure, more Na^+ ions are needed as the "gluing" agent between adjacent AOT. This hypothesis is supported by the fact that triply charged micellar ions generally are more stable and have higher intensities than doubly charged ions, as shown in Fig. 2b.

4.2. Is water necessary for reverse micelles?

One unique feature of solution-phase reverse micelles is the existence of confined, ordered water molecules inside the micellar core [61–64]. Nanoscale water droplets are assumed to promote the aggregation of amphiphilic surfactants around the micellar core. Surprisingly, water molecules are absent in most gas-phase reverse micellar ions, with the exception of small aggregates where n = 2–5, in which a progression of water adducts were formed. We also found loss of water from gas-phase reverse micelles which incorporate Gly molecules. As demonstrated in present and previous experiments [21,24,25], losing water does not affect the stability of gas-phase NaAOT reverse micelles. Theoretical simulations [21,29] also suggest that the stability of reverse micellar structure in the vacuum is independent of water. Moreover, the structure of a dry, isolated AOT reverse micelle with a central void has been proposed by direct optimization [31].

Loss of water was also observed in gas-phase CTAB reverse micelles [22] and in other biological complexes (i.e., structural waters) [65] and was interpreted in terms of dissociation upon collisions [22]. While collision activated dissociation could be a main reason for water loss, other factors may also contribute to the loss of water molecules initially confined in the interior of reverse micelles. We noticed that Flynn and co-workers reported NMR studies of low temperature-induced water shedding from NaAOT reverse micelles composed of a low ionic strength aqueous core [66,67]. They explained that encapsulation of water molecules into NaAOT reverse micelles is a spontaneous process. Since insertion of water in NaAOT reverse micelles is an endothermic process (unfavorable from an enthalpic point of view), the positive change of the system enthalpy (ΔH) must be compensated by a positive change of the system entropy (ΔS) [67–69]. As temperature decreases and water becomes supercooled, enthalpy dominates the system and the micelles expel water. Since in ESI experiments evaporation of solvent from electrospray droplets also results in cooling of reverse micelles before they enter the capillary, we tentatively assign the low temperature as one of possible factors prompting loss of internal water in the micellar core. As water sheds, the size of the reverse micelles naturally decreases, leading to stronger interactions between Na^+ ions and sulfonate/carbonyl groups of AOT.

4.3. Encapsulation of amino acids into gas-phase reverse micelles

How are Gly molecules entrapped in gas-phase NaAOT reverse micelles? Gly could be randomly attached to the micellar surface, or entangled with AOT hydrophobic tails. However, these possibilities may be discounted for several reasons. First, Gly is a very hydrophilic molecule and would be expected to partition more strongly into the micellar core than the hydrophobic interface. Secondly, both formation and CID of reverse micellar ions encapsulating Gly demonstrate a strong dependence on size for encapsulation, and only reverse micelles of $n \geq 13$ are able to host a Gly (therefore proving that it is not attached to the micellar surface). Finally, if Gly is attached to the outer surface of reverse micelles, we would have observed product ions corresponding to stripping Gly, and only Gly, off the precursor ions. However, we did not observe such product ions from CID. In fact, expelling of Gly from micelles always results in a breakdown of the whole micellar structure. We did notice that in Fig. 6 there are minor peaks at the mass/charge positions corresponding to empty precursor ions, however, these ion signals are artificial (contaminants from the ion source due to the low mass resolution we set for the first quadrupole mass filter). Therefore, it is more convincing that Gly is encapsulated inside the micellar core.

5. Conclusions

We have presented the formation and characterization of multiply charged NaAOT reverse micelles in the gas phase using ESI guided-ion beam tandem mass spectrometry. It was found that, under the same experimental conditions, different ESI solutions result in dramatic differences in the size and charge distributions of gas-phase reverse micelles. For example, ESI of a NaAOT (5.0×10^{-3} M)/water (ω_0 = 10)/hexane micellar solution produces a wide spectrum of species characterized by $[(NaAOT)_nNa_z]^{z+}$ with n in the range of 2–44 and z in the range of 1–5. ESI of NaAOT monomers in hexane or methanol/water, on the other hand, produces relatively small micelles in low charge states. The dependence of gas-phase reverse micelle sizes and charges on starting solutions suggests that, in addition to self-assembling of surfactants in the gas-phase, pre-formed micelles in solution may preserve reverse micellar structure when transferred to the gas phase (at least to some extent) and thus help form large gas-phase aggregates. Surprisingly, we found no water present in gas-phase reverse micelles, contrary to the general view that reverse micelle requires water molecules to "glue" the assembly. We speculate that, because of water shedding, more Na^+ are required to coordinate with AOT and support the reverse micellar structure. This finding may lead to potential applications of gas-phase reverse micelles in synthetic tasks where the absence of water is required for extremely aggressive chemistry [70]. Another most interesting finding from our experiment is that gas-phase NaAOT reverse micelles could encapsulate Gly molecules, and thus act as nanometer-sized carriers of biomolecules in the gas phase. Encapsulation of Gly appears to be strongly micelle size dependent, indicating that Gly molecules

are most likely located in the hydrophilic interior of the micelles. CID has been investigated for both empty and Gly-encapsulating reverse micellar ions, including measurements of product ions and CID cross-sections over a center-of-mass E_{col} range of 0.1–8.0 eV. CID results provide insights into gas-phase reverse micellar structures and stability, as well as their dependence on micelle size, charge and encapsulations.

Our experimental results are in agreement with previous theoretical modeling of gas-phase reverse micelles [29,31]. However, some interesting questions remains, particularly regarding the driving forces for aggregation of NaAOT, multiple charges, water shedding and interactions of encapsulated amino acids with surfactants. We hope the present experimental measurements will stimulate interest in theoretical modeling to sharpen a microscopic picture of multiply charged gas-phase reverse micellar structure.

Acknowledgements

This work was supported by the Donors of the American Chemical Society Petroleum Research Fund (PRF #48208-G6), CUNY Collaborative Grant, Queens College Research Enhancement Funds and PSC-CUNY Research Awards. Y.F. is the recipient of the CUNY Doctoral Student Research Grant in 2010. A.B. acknowledges support by Queens College Undergraduate/Mentoring Education Initiative.

References

[1] P.L. Luisi, M. Giomini, M.P. Pileni, B.H. Robinson, Biochim. Biophys. Acta 947 (1988) 209.
[2] M.P. Pileni, Studies in Physical and Theoretical Chemistry 65: Structure and Reactivity in Reverse Micelles, Elsevier Science Publishers, Amsterdam, 1989.
[3] K. Kon-no, Surf. Colloid Sci. 15 (1993) 125.
[4] R.W. Gale, J.L. Fulton, R.D. Smith, J. Am. Chem. Soc. 109 (1987) 920.
[5] V.T. Liveri, Nano-Surf. Chem. (2002) 473.
[6] A.M. Middlebrook, D.M. Murphy, D.S. Thomson, J. Geophys. Res. 103 (1998) 16475.
[7] D.M. Murphy, D.S. Thomson, M.J. Mahoney, Science 282 (1998) 1664.
[8] G.B. Ellison, A.F. Tuck, V. Vaida, J. Geophys. Res. 104 (1999) 11633.
[9] H. Tervahattu, K. Hartonen, V.-M. Kerminen, K. Kupiainen, P. Aarnio, T. Koskentalo, A.F. Tuck, V. Vaida, J. Geophys. Res. 107 (2002) 4053.
[10] H. Tervahattu, J. Juhanoja, K. Kupiainen, J. Geophys. Res. 107 (2002) 4319.
[11] P.S. Gill, T.E. Graedel, C.J. Weschler, Rev. Geophys. Space Phys. 21 (1983) 903.
[12] C.M. Dobson, G.B. Ellison, A.F. Tuck, V. Vaida, PNAS 97 (2000) 11864.
[13] D.J. Donaldson, A.F. Tuck, V. Vaida, Phys. Chem. Chem. Phys. 3 (2001) 5270.
[14] G. Siuzdak, B. Bothner, Angew. Chem. Int. Ed. 34 (1995) 2053.
[15] D. Nohara, T. Ohkoshi, T. Sakai, Rapid Commum. Mass Spectrom. 12 (1995) 1933.
[16] D. Nohara, M. Bitoh, J. Mass Spectrom. 35 (2000) 1434.
[17] F. Cacace, G. de Petris, E. Giglio, F. Punzo, A. Troiani, Chem. Eur. J. 8 (2002) 1925.
[18] C.L. Hanson, L.L. Ilag, J. Malo, D.M. Hatters, J. Geoffrey, C.V. Howlett, Robinson, Biophys. J. 85 (2003) 3802.
[19] L.L. Ilag, I. Ubarretxena-Belandia, C.G. Tate, C.V. Robinson, J. Am. Chem. Soc. 126 (2004) 14362.
[20] D. Nohara, T. Kajiura, K. Takeda, J. Mass Spectrom. 40 (2005) 489.
[21] D. Bongiorno, L. Ceraulo, A. Ruggirello, V.T. Liveri, E. Basso, R. Seraglia, P. Traldi, J. Mass Spectrom. 40 (2005) 1618.
[22] M. Sharon, L.L. Ilag, C.V. Robinson, J. Am. Chem. Soc. 129 (2007) 8740.
[23] N.P. Barrera, N.D. Bartolo, P.J. Booth, C.V. Robinson1, Science 321 (2008) 243.
[24] G. Giorgi, L. Ceraulo, V.T. Liveri, J. Phys. Chem. B (2008) 1376.
[25] G. Giorgi, E. Giocaliere, L. Ceraulo, A. Ruggirello, V.T. Liveri, Rapid Commun. Mass Spectrom. 23 (2009) 2206.
[26] G. de Petris, M.R. Festa, L. Galantini, E. Giglio, C. Leggio, N.V. Pavel, A. Troiani, J. Phys. Chem. B 113 (2009) 7162.
[27] M. Yamashita, J.B. Fenn, J. Phys. Chem. 88 (1984) 4451.
[28] J.B. Fenn, M. Mann, C.K. Meng, S.F. Wong, C.M. Whitehouse, Science 246 (1989) 64.
[29] Y. Wang, D.S.D. Larsson, D.v.d. Spoel, Biochemistry 48 (2009) 1006.
[30] R. Allen, S. Bandyopadhyay, M.L. Klein, Langmuir 16 (2000) 10547.
[31] A.I. Bulavchenko, A.F. Batishchev, E.K. Batishcheva, V.G. Torgov, J. Phys. Chem. B 106 (2002) 6381.
[32] R. Neutze, R. Wouts, D.v.d. Spoe, E. Weckert, J. Hajdu, Nature 406 (2000) 752.
[33] Y. Fang, J. Liu, J. Phys. Chem. A 113 (2009) 11250.
[34] D. Gerlich, in: C.Y. Ng, M. Baer (Eds.), State-Selected and State-To-State Ion–Molecule Reaction Dynamics. Part i. Experiment, 82, John Wiley & Sons, Inc., New York, 1992, p. p. 1.
[35] K. Mukherjee, S.P. Moulik, D.C. Mukherjee, Langmuir 9 (1993) 1727.
[36] J.F.D.L. Mora, J. Fluid Mech. 243 (1992) 561.
[37] J.S. Klassen, Y. Ho, A.T. Blades, P. Kebarle, Adv. Gas-Phase Ion Chem. 3 (1998) 255.
[38] P. Kebarle, J. Mass Spectrom. 35 (2000) 804.
[39] S.E. Rodriguez-Cruz, J.T. Khoury, J.H. Parks, J. Am. Soc. Mass Spectrom. 12 (2001) 716.
[40] S.K. Chowdhury, V. katta, B.T. Chait, Rapid Commun. Mass Spectrom. 4 (1990) 81.
[41] T. Kim, K. Tang, H.R. Udseth, R.D. Smith, Anal. Chem. 73 (2001) 4162.
[42] K. Tang, A.V. Tolmachev, E. Nikolaev, R. Zhang, M.E. Belov, H.R. Udseth, R.D. Smith, Anal. Chem. 74 (2002) 5431.
[43] R.M. Moision, P.B. Armentrout, J. Am. Soc. Mass Spectrom. 18 (2007) 1124.
[44] A.N. Krutchinsky, I.V. Chernushevich, V.L. Spicer, W. Ens, K.G. Standing, J. Am. Soc. Mass Spectrom. 9 (1998) 569.
[45] D.J. Douglas, J.B. French, J. Am. Mass Spectrom. 3 (1992) 398.
[46] K.M. Ervin, P.B. Armentrout, J. Chem. Phys. 83 (1985) 166.
[47] S.A. McLuckey, G.L. Glish, G.J.V. Berkel, Anal. Chem. 63 (1991) 1971.
[48] J. James, L. Stephenson, S.A. McLuckey, Anal. Chem. 70 (1998) 3533.
[49] G. Wang, R.B. Cole, in: R.B. Cole (Ed.), Electrospray Ionization Mass Spectrometry: Fundamentals, Instrumentation, and Applications, John Wiley & Sons, Inc., New York, 1997, p. p. 137.
[50] M. Ueda, Z.A. Schelly, J. Colloid Interface Sci. 124 (1988) 673.
[51] M. Ueda, Z.A. Schelly, Langmuir 4 (1988) 653.
[52] M.E. Leser, P.L. Luisi, Chimia 44 (1990) 270.
[53] A.M. Maitra, P.K. Patanjali, in: K.L. Mittal, P. Bothorel (Eds.), Surfactants in Solution, 5, Plenum Press, New York, 1986, p. p. 581.
[54] R.M. Lemert, R.A. Fuller, K.P. Johnston, J. Phys. Chem. 94 (1990) 6021.
[55] R.M. Moision, P.B. Armentrout, J. Phys. Chem. A 106 (2002) 10350.
[56] S.J. Ye, R.M. Moision, P.B. Armentrout, Int. J. Mass Spectrom. 240 (2005) 233.
[57] J. Liu, B. Van Devener, S.L. Anderson, J. Chem. Phys. 116 (2002) 5530.
[58] J. Faeder, B.M. Ladanyi, J. Phys. Chem. B 104 (2000) 1033.
[59] J. Chowdhary, B.M. Ladanyi, J. Phys. Chem. B 113 (2009) 15029.
[60] M.J. Frisch, G.W. Trucks, H.B. Schlegel, G.E. Scuseria, M.A. Robb, J.R. Cheeseman, J.J.A. Montgomery, T. Vreven, K.N. Kudin, J.C. Burant, J.M. Millam, S.S. Iyengar, J. Tomasi, V. Barone, B. Mennucci, M. Cossi, G. Scalmani, N. Rega, G.A. Petersson, H. Nakatsuji, M. Hada, M. Ehara, K. Toyota, R. Fukuda, J. Hasegawa, M. Ishida, T. Nakajima, Y. Honda, O. Kitao, H. Nakai, M. Klene, X. Li, J.E. Knox, H.P. Hratchian, J.B. Cross, V. Bakken, C. Adamo, J. Jaramillo, R. Gomperts, R.E. Stratmann, O. Yazyev, A.J. Austin, R. Cammi, C. Pomelli, J.W. Ochterski, P.Y. Ayala, K. Morokuma, G.A. Voth, P. Salvador, J.J. Dannenberg, V.G. Zakrzewski, S. Dapprich, A.D. Daniels, M.C. Strain, O. Farkas, D.K. Malick, A.D. Rabuck, K. Raghavachari, J.B. Foresman, J.V. Ortiz, Q. Cui, A.G. Baboul, S. Clifford, J. Cioslowski, B.B. Stefanov, G. Liu, A. Liashenko, P. Piskorz, I. Komaromi, R.L. Martin, D.J. Fox, T. Keith, M.A. Al-Laham, C.Y. Peng, A. Nanayakkara, M. Challacombe, P.M.W. Gill, B. Johnson, W. Chen, M.W. Wong, C. Gonzalez, J.A. Pople, Gaussian 03, rev E. 01, Gaussian, Inc., Wallingford, CT, 2004.
[61] M. Wong, J.K. Thomas, T. Nowak, J. Am. Chem. Soc. 99 (1977) 4730.
[62] H.-S. Tan, I.R. Piletic, M.D. Fayer, J. Chem. Phys. 122 (2005) 174501.
[63] M.R. Harpham, B.M. Ladanyi, N.E. Levinger, J. Phys. Chem. B 109 (2005) 16891.
[64] P.A. Pieniazek, Y.-S. Lin, J. Chowdhary, B.M. Ladanyi, J.L. Skinner, J. Phys. Chem. B 113 (2009) 15017.
[65] S.-W. Lee, P. Freivogel, T. Schindler, J.L. Beauchamp, JACS 120 (1998) 11758.
[66] W.D.V. Horn, A.K. Simorellis, P.F. Flynn, J. Am. Chem. Soc. 127 (2005) 13553.
[67] A.K. Simorellis, W.D.V. Horn, P.F. Flynn, J. Am. Chem. Soc. 128 (2006) 5082.
[68] A. D'Aprano, A. Lizzio, V.T. Liveri, J. Phys. Chem. 91 (1987) 4749.
[69] S.P. Moulik, S. Ray, Pure Appl. Chem. (1994) 3.
[70] J.P. Wilcoxon, P.P. Provencio, J. Phys. Chem. B 103 (1999) 9809.